Majorana Corner Modes with Solitons in an Attractive Hubbard-Hofstadter Model of Cold Atom Optical Lattices

Chuanchang Zeng,[1] T. D. Stanescu,[2] Chuanwei Zhang,[3] V. W. Scarola,[4] and Sumanta Tewari[1]
[1]Department of Physics and Astronomy, Clemson University, Clemson, South Carolina 29634, USA
[2]Department of Physics and Astronomy, West Virginia University, Morgantown, West Virginia 26506, USA
[3]Department of Physics, The University of Texas at Dallas, Richardson, Texas 75080, USA
[4]Department of Physics, Virginia Tech, Blacksburg, Virginia 24061, USA

(Received 8 February 2019; published 6 August 2019)

Higher-order topological superconductors hosting Majorana-Kramers pairs (MKPs) as corner modes have recently been proposed in a two-dimensional quantum spin Hall insulator proximity-coupled to unconventional cuprate or iron-based superconductors. Here, we show that such MKPs can be realized using a conventional s-wave superfluid with a soliton in cold atom systems governed by the Hubbard-Hofstadter model. The MKPs emerge in the presence of interaction at the "corners" defined by the intersections of line solitons and the one-dimensional edges of the system. Our scheme is based on the recently realized cold atom Hubbard-Hofstadter lattice and will pave the way for observing possible higher-order topological superfluidity with conventional s-wave superfluids or superconductors.

DOI: 10.1103/PhysRevLett.123.060402

Introduction.—D-dimensional topological insulators or superconductors (TI-TS) are characterized by a fully gapped bulk spectrum and stable gapless conducting states localized on $(D-1)$-dimensional boundaries [1,2]. Examples include the 3D strong TI with an odd number of gapless Dirac cones localized on 2D surfaces and the 1D spinless p-wave superconductors (SCs) with zero-dimensional Majorana zero modes (MZMs) localized near the end points of the system. By contrast, the recently introduced so-called higher-order TIs and TSs are gapped in the bulk as well as on the $(D-1)$-dimensional boundary but have robust gapless topological modes on $(D-2)$-dimensional "edges" defined on the boundary, e.g., corners in 2D systems and hinges in 3D systems. This idea has been used to explain the existence of protected low-energy corner modes in 2D quantized electric quadrupole insulators [3–11] and the existence of 1D protected gapless hinge modes in 3D crystals of bismuth [12].

It has been recently proposed [13–15] that zero-dimensional Majorana corner modes (MCMs) in 2D SC systems can be realized from a combination of 2D TI [quantum spin Hall insulator (QSHI)] and unconventional (non-s-wave) superconductors. Excitations in these systems come in the form of MKPs, which are distinct from nondegenerate MZMs [16–26] and are protected by time-reversal (TR) symmetry [27–46]. Unfortunately, MCMs proposed in the condensed matter systems [13–15,47–51] have not been realized to date.

In this Letter, we propose ultracold atoms in optical lattices as a clean and straightforward route to realize MCMs and higher-order topological superfluidity with ordinary s-wave superfluids. 2D QSHI Hamiltonians have now been experimentally realized in cold atom systems on square optical lattices [52]. These systems are accurately modeled by a two-component Hofstadter model in a TR-invariant scheme where the atoms experience opposite uniform magnetic fields for each of the two components [52–59]. Furthermore, s-wave superfluidity can be induced with an attractive Hubbard interaction arising from a Feshbach resonance between the fermions [60–66]. Specifically, we study a 2D TR-invariant Hofstadter model H_0, with an attractive Hubbard interaction H_I: $H = H_0 + H_I$. The model is characterized by an interaction-controlled phase transition between a QSHI and a superfluid (SF). Above a critical value of the attractive interaction, both the edge and the bulk have a nonzero superfluid order parameter due to BCS-like pairing. Since the edge spectrum is gapped, the 2D superfluid is topologically trivial, according to the conventional (lower-order) bulk-boundary correspondence. We show, however, that the superfluid can host MKPs when a line soliton intersects the edges, changing the sign of the superfluid order parameter [14,15]. Dark solitons [67], which have been successfully observed recently in Fermi gases [68–70] using phase imprinting [71], can arise as topological defects where the order parameter vanishes and the phase changes by π [72,73]. Intuitively, the edge states are gapped by the superfluid order parameter, which acts as a Dirac mass. At the intersection of the dark line soliton with the sample edges, the superfluid order parameter (and, hence, the Dirac mass) changes sign, producing a pair of localized zero-dimensional MZMs protected by TR symmetry. Tunneling into the soliton edges can be used to observe these MKPs [72]. We emphasize that the uniform

superfluid with no soliton is topologically trivial (in the conventional sense), with the appropriate $\mathcal{Z}_2$ invariant [74] being trivially zero because of the absence of gapless edge modes. Therefore, our work proposes the first cold-atom-based realization of $(D-2)$-dimensional MZMs in what is a D-dimensional topologically trivial system in the conventional sense and is thus an experimentally realizable higher-order topological superfluid.

Noninteracting model and Hofstadter bands.—The Hofstadter model [54] describes noninteracting particles on a 2D lattice in the presence of a perpendicular magnetic field $\boldsymbol{B} = B\hat{z}$ given by the vector potential $\boldsymbol{A} = (0, Bx, 0)$. We consider a generalization of the original model that includes a spin-dependent magnetic field:

$$H_0 = -\sum_{i,j,\sigma}[t_x c^\dagger_{i,j,\sigma}c_{i+1,j,\sigma} + t^\sigma_y(i)c^\dagger_{i,j,\sigma}c_{i,j+1,\sigma} + \text{H.c.}] + \sum_{i,j,\sigma}(V_{i,j}-\mu)c^\dagger_{i,j,\sigma}c_{i,j,\sigma}, \quad (1)$$

where (i,j) labels the sites of a square lattice with lattice constant a, $c^\dagger_{i,j,\sigma}$ ($c_{i,j,\sigma}$) creates (annihilates) a particle at (i,j) with spin $\sigma \equiv \{\uparrow,\downarrow\}$, and $t_x = t$ and $|t^\sigma_y(i)| = t$ are nearest-neighbor hopping amplitudes along the x and y directions, respectively. We set $t = 1$ and consider (i) periodic boundary conditions, (ii) a cylindrical geometry (periodic in the y direction and a finite width in the x direction, $L_x = aN_x$), and (iii) a rectangular geometry with $L_x = aN_x$, $L_y = aN_y$. The chemical potential is μ, while $V_{i,j}$ is a position-dependent confinement potential (see Supplemental Material [75]).

In the presence of the (spin-dependent) magnetic field, the hopping amplitude $t^\sigma_y(i)$ acquires a spin- and x-dependent phase factor $e^{i2\pi\phi_{x_i,\sigma}}$, with $\phi_{x_i,\sigma} = s_\sigma eBax_i/h$. Here, $x_i = ia$ is the position along the x direction, while $s_\uparrow = 1$ and $s_\downarrow = -1$ correspond to opposite magnetic field orientations for the two spin components, which explicitly restores TR symmetry, in contrast with the original Hofstadter model. We define the number of magnetic-flux quanta per unit cell as $\alpha = (Ba^2)/\phi_0$, with $\phi_0 = h/e$ the magnetic-flux quantum, and we have $t^\sigma_y(\ell) = te^{s_\sigma i2\pi\alpha\ell}$. For $\alpha = p/q$, with p and q primes, the single-particle energy spectrum is given by q subbands $\epsilon_{\mathbf{k}n}$, with $n = 0,1,2,\ldots,q-1$. Here, we focus on the case $\alpha = 1/3$. We expect similar physics for other values of α that support QSHI phases.

In momentum space, $\mathbf{k} = (k_x, k_y)$, Eq. (1) with $\alpha = 0$ can be written as $H_0(\boldsymbol{k}) = -2t\sum_{k_x,k_y,\sigma}[\cos(k_x) + \cos(k_y)]$. The corresponding energy spectrum has a bandwidth of $8t$, and the system is topologically trivial. To explore a topologically nontrivial regime, we consider $\alpha = 1/3$ and use the Fourier transform $c_{i,j,\sigma} = N_0^{-1/2}\sum_k e^{i\mathbf{kr}}c_{k,\beta,\sigma}$, where $\mathbf{r} = (i,j)$ and N_0 is the total number of lattice sites. The field-induced phase factors contained in $t^\sigma_y(\ell)$ give rise to a new periodicity in the x direction: $e^{i2\pi s_\sigma\alpha\ell} = 1, e^{i2\pi s_\sigma/3}, e^{i4\pi s_\sigma/3}$ for $\ell \bmod 3 = 0,\ 1,\ 2$, respectively. We label the nonequivalent sites in the nth magnetic unit cell as $\beta = 0,\ 1,\ 2$, and we have $x_\ell/a = \ell(n,\beta) = nq + \beta$. The corresponding first Brillouin zone is $k_x \in [-\pi/q, \pi/q]$ and $k_y \in [-\pi,\pi]$. After Fourier transforming, we can rewrite H_0 as

$$H_0(\mathbf{k}) = \sum_{\mathbf{k}\sigma}\psi^\dagger_{\mathbf{k},\sigma}\begin{pmatrix} h_0 & e^{ik_y} & e^{-ik_y} \\ e^{-ik_y} & h_1 & e^{ik_y} \\ e^{ik_y} & e^{-ik_y} & h_2 \end{pmatrix} \otimes I_2\psi_{\mathbf{k},\sigma}, \quad (2)$$

where I_n is the $n\times n$ identity matrix, $\mathbf{k}_\beta = (k_x - \beta 2\pi\alpha, k_y)$, $\psi_{\mathbf{k},\sigma} = (c_{\mathbf{k}_1,\sigma}, c_{\mathbf{k}_2,\sigma}, c_{\mathbf{k}_3,\sigma})^T$, and $h_\beta = 2\cos(k_x - 2\pi\beta\alpha)$, with $\beta = 0,\ 1,\ 2$. The corresponding band structure is characterized by $q = 3$ spin-degenerate bands with nonzero Berry curvature $\Omega^\sigma_{\mathbf{k}}$ and a nonzero spin-dependent Chern number. Although the total Chern number of a fully filled band is zero due to TR symmetry [82], the corresponding $\mathcal{Z}_2$ invariant reveals a topological-nontrivial QSHI phase. The characteristic edge modes can be obtained using a cylindrical geometry with periodic boundary conditions in the y direction. The corresponding band structure for a system with both hard and soft confinement [75] is shown in Fig. 1. The red lines indicate the (confinement-dependent) gapless edge states, while the (dense) blue lines correspond to the bulk spectrum. When the chemical potential intersects the red lines, e.g., at $\pm\mathbf{k}_\sigma$, the system supports a pair of gapless edge states $(\mathbf{k}_\uparrow, -\mathbf{k}_\downarrow)$ located along one of the edges and another pair $(-\mathbf{k}_\uparrow, \mathbf{k}_\downarrow)$ located on the other edge. Consequently, if μ lies within a bulk gap, the system is in a topological QSHI phase with pairs of counterpropagating gapless modes located along the edges.

Attractive interactions.—Next, we introduce an attractive interaction described in real space by the Hubbard term

$$H_I = -U\sum_{i,j} n_{i,j,\uparrow}n_{i,j,\downarrow}, \quad (3)$$

where $U > 0$ is the magnitude of the on-site attraction. In cold atom systems, the interaction can derive from an attractive Feshbach resonance [63,66]. We study the effect of this attractive interaction at the mean-field level using a BCS-like approximation. In k space, we have

$$H_I \to \sum_{\mathbf{k},\beta}(\Delta^\dagger c_{-\mathbf{k},\beta\downarrow}c_{\mathbf{k},\beta\uparrow} + \Delta c^\dagger_{\mathbf{k},\beta\uparrow}c^\dagger_{-\mathbf{k},\beta\downarrow}) + \frac{3N_0}{U}|\Delta|^2, \quad (4)$$

where we have introduced a uniform [83] order parameter $\Delta = -(U/N_0)\sum_{\mathbf{k}}\langle c_{-\mathbf{k},\beta\downarrow}c_{\mathbf{k},\beta\uparrow}\rangle$, with $\langle\cdots\rangle$ indicating the thermal average. At this mean-field level, the total Hamiltonian becomes

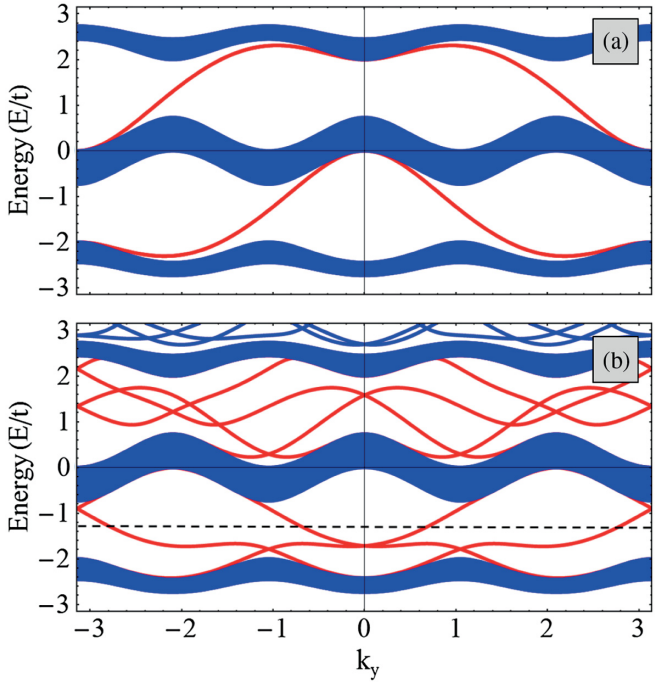

FIG. 1. Band structure of the noninteracting two-component Hofstadter model H_0, with $\alpha = 1/3$ and periodic boundary conditions in the y direction. (a) System with $N_x = 92$ and hard confinement in the x direction. (b) System with $N_x = 92$ and soft (Gaussian) confinement (see Supplemental Material [75]). The bulk states are shown in blue, and the red curves represent the gapless edge modes.

$$H_{\mathrm{MF}} = \sum_{\mathbf{k}} \Psi_{\mathbf{k}}^{\dagger} \begin{pmatrix} h_B(\mathbf{k}) - \mu & \Delta \cdot I_3 \\ \Delta^{\dagger} \cdot I_3 & -h_B^*(-\mathbf{k}) + \mu \end{pmatrix} \Psi_{\mathbf{k}} + \mathcal{E}, \qquad (5)$$

where $\Psi_{\mathbf{k}} = (\psi_{\mathbf{k},\uparrow}, \psi_{-\mathbf{k},\downarrow}^{\dagger})^T$, h_B is the matrix in Eq. (2), and $\mathcal{E} = -\sum_{\mathbf{k}} (3\mu - 3|\Delta|^2/U + \mathbf{Tr} E_{-\mathbf{k},\downarrow})$ is an energy offset. We solve this model using a self-consistent BCS-like formalism outlined in Supplemental Material [75].

The mean-field phase diagram corresponding to Eq. (5) is shown in Fig. 2. When the chemical potential lies within the bulk gap, the self-consistent value of the s-wave pairing becomes nonzero only above a finite interaction strength $U_c(\mu)$. For $U < U_c(\mu)$, the system is in a QSHI phase with $\Delta = 0$, while $U > U_c(\mu)$ corresponds to the superfluid phase ($\Delta \neq 0$). Note that, for $\mu \in [-2t, -0.7t]$, the phase transition from a QSHI state with filling factor $n_0 = 2/3$ to the SF state occurs at a critical interaction on the order of $3t$. On the other hand, at half filling ($n_0 = 1$), $\Delta \neq 0$ for any finite U and the system is in a SF phase. Below, we will show that the SF phase supports MKPs in the presence of a line soliton, when the order parameter changes sign.

Soliton-induced Majorana zero-energy modes.—Next, we show that, in the presence of a line soliton, MKPs emerge at the "corners" defined by the intersection of the soliton with the edge of the system, which is in a TR symmetric SF phase. In the presence of a dark soliton, the order parameter changes

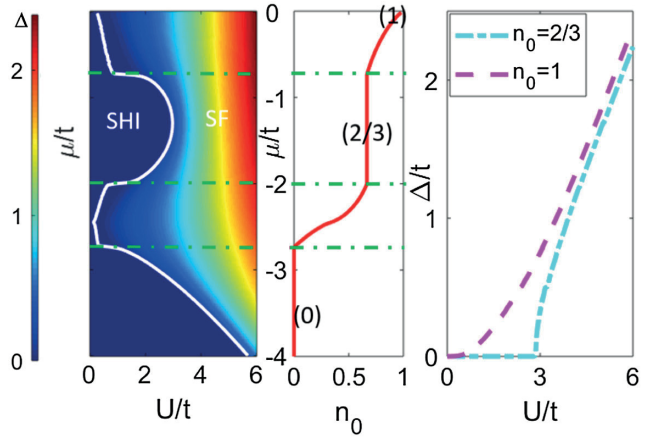

FIG. 2. Left: The mean-field phase diagram obtained by plotting the self-consistent value of the pairing order parameter Δ for $k_B T = 10^{-4} t$. The dashed white line indicates the phase boundary. Center: Chemical potential as a function of the filling factor for $\Delta = 0$. Right: Mean-field Δ as a function of the interaction strength for two different filling factors. The $n_0 = 1$ line shows $\Delta \neq 0$ (i.e., superfluid phase) all the way to $U \sim 0$, while for $n_0 = 2/3$ one needs $U \sim 3t$ to enter the superfluid phase. The green dotted lines mark the band edges of the bulk spectrum in Fig. 1.

sign, vanishing along a node line. To study the impact of the soliton, we construct the Bogoliubov–de Gennes (BdG) equations in real space and solve them self-consistently [75]. We choose the initial value of the order parameter to be used in the self-consistent scheme as $\tilde{\Delta}_{i,j} = \Delta_{i,j} \tanh[(i - 28 + 5\cos[(j-1)\pi/(N_y - 1)])/\xi]$, where $\Delta_{i,j}$ is a constant phase self-consistent solution (i.e., obtained without the soliton) and $\xi = 2.5$. We then solve the BdG equations for $N_x \times N_y = 50 \times 34$ sites and $n_0 = 2/3$.

In Fig. 3, we show the self-consistent solution for $\Delta(x, y)$ for a system with $U = 3.5t$ without a soliton (top) and with a line soliton (bottom). Note that $U > U_c(\mu)$, so that, without the soliton, the system is in a SF phase with a nonvanishing order parameter both in the bulk and on the edge. The bottom panel shows that the soliton changes the sign of the order parameter, as expected. Note that for $U < U_c(\mu)$ the order parameter vanishes in the bulk but remains finite on the edge, where it changes sign in the presence of a soliton (see Supplemental Material [75]).

The low-energy spectra corresponding to the self-consistent solutions in Fig. 3 are shown in Fig. 4. The top panel (no soliton) is characterized by a finite quasiparticle gap and low-energy states located along the edges of the system (see the inset). The bottom panel, corresponding to a system with a soliton, has four zero-energy states (red circles) representing the MKPs. As shown in the inset, the corresponding wave functions are localized at the intersection of the line soliton with the edges of the system.

Our results show that MKPs can be induced at soliton edges in a conventional s-wave SF. We have checked that

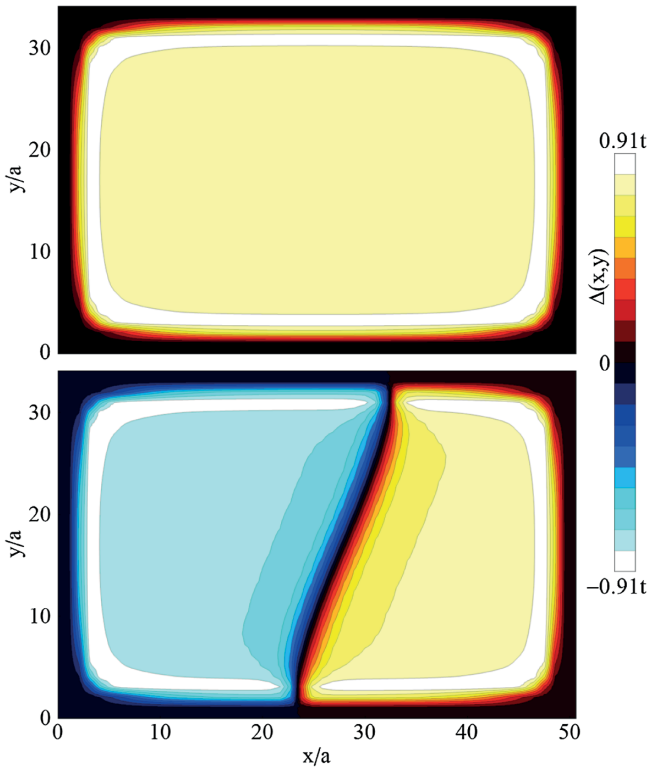

FIG. 3. Position-dependent pairing potential $\Delta(x, y)$ for a strongly interacting system with $U = 3.5t$, i.e., in the SF phase. The pairing potential is obtained as the self-consistent solution of the mean-field equations (Eqs. S7–S10) for a finite system with $N_x \times N_y = 50 \times 34$ and soft confinement (see Supplemental Material [75]) at finite temperature $k_B T = 0.01t$. The total number of particles is fixed: $N = 800$. Top: Self-consistent solution with a constant phase. The (self-consistent) chemical potential is $\mu = -1.250t$. Bottom: Self-consistent solution with a line soliton. The chemical potential is $\mu = -1.248t$. Note that $\Delta(x, y)$ is nonzero in the bulk—consistent with the phase diagram in Fig. 2(b)—as well as on the boundary of the system, except along the line soliton.

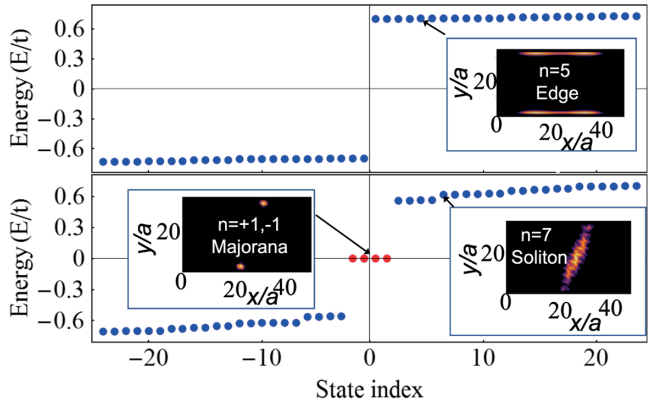

FIG. 4. Top: Low-energy spectrum of the Hofstadter-Hubbard model with a strong interaction ($U = 3.5t$) within the mean-field approximation for a system with constant phase pairing potential and parameters corresponding to Fig. 3 (top). Bottom: The same but for parameters corresponding to the bottom panel in Fig. 3. Note that in the presence of a line soliton the system hosts two pairs of zero-energy Majorana bound states (red dots). The insets plot the wave functions of the states marked by arrows.

the line soliton and the corresponding MKPs are robust against small perturbations (e.g., thermal fluctuations and on-site disorder; see Supplemental Material [75]) and are thus topologically robust.

Implementation.—To implement H_0, we envision an experimental setup similar to Ref. [52], since this scheme does not rely on the internal atomic structure. We consider a 3D cubic optical lattice where confinement along z separates the system into parallel x–y planes. The 2D Hubbard model then approximates the dynamics of ^{40}K or ^{6}Li placed with one atom per site in a deep optical lattice with uniform hopping t if we equally populate two Zeeman levels with opposite magnetic moments. A magnetic field gradient along the y direction creates a splitting (much larger than t) between opposite spins in neighboring sites. In addition to the primary lattice beams, a pair of running-wave beams are applied parallel to the $x - y$ bonds of the square lattice to dynamically restore resonant tunneling, assuming the running-wave lattice depth is much smaller than the spin splitting. This setup induces the complex spin-dependent phase in Eq. (1) in a rotating wave approximation.

To implement H_I, we require an attractive Feshbach resonance. For magnetic Feshbach resonances, typical magnetic field gradients ($\sim$10 mG/μm) leave the attractive interaction spatially uniform, since common resonances occur at relatively high fields ($\sim$400–700 G) and can be broad, as in, e.g., ^{6}Li. It also safe to assume that close proximity to the Feshbach resonance does not lead to strong heating and loss [84], since the Raman coupling [52] between the same hyperfine states (and neighboring lattice sites) does not induce any new three-body loss channel.

Tuning the chemical potential near zero (Fig. 4) allows observation of MZMs. Spatially resolved radio-frequency spectroscopy and probing of the density profile have been proposed as an experimental approach to detect these MZMs [73,76]. The soliton-induced MZMs can be manipulated by controlling the spatial location of the soliton excitation, which may be beneficial for topological braiding [85,86] of MZMs.

Discussion and conclusion.—The essential physics for the creation of MKPs and higher-order topological superfluidity in the current system is similar to the proposals for higher-order topological superconductors in solid state systems. In both cases, the non-SC "normal" system is a 2D QSHI. This system has counterpropagating Kramers pairs of gapless edge states (see Fig. 1), which can support spin-singlet superconductivity. Furthermore, in both systems, introducing superconductivity (by the proximity effect in solid state systems and interaction induced, via Feshbach resonance, in the present work) gaps out the edge modes, which signals that the system is a topologically trivial superconductor or superfluid (because

the edge modes are gapped). However, whenever the superconducting gap changes sign (and, thus, goes through zero) at a point along the edge, a Kramers pair of localized MZMs are nucleated by the Jackiew-Rebbi mechanism, which is common to both the solid state proposals and the present work (a Kramers pair of zero modes is nucleated because the system is time-reversal invariant).

The key difference between the solid state case and the current setup is that in the former system the change of sign of the superconducting gap is proposed to be realized by the proximity effect with an unconventional superconductor (such as d wave or $s_{\pm}$ wave, which change sign in momentum space), while in our work the change of sign of the superconducting gap is due to a soliton in the s-wave superfluid. The other significant difference between the two proposals is that, while the proximity effect of unconventional d- or $s_{\pm}$-wave superconductivity on QSHI in solid state systems has not yet been demonstrated experimentally (and is probably going to be hard), the main ingredients of the same physics within our proposal, namely, the two-component Hofstadter model (and, thus, a QSHI [52–59]), on-site attractive interactions and nonzero SC pair potential [60–66], and creation of dark solitons [67–70], have all been individually realized in the cold atom systems.

C. Z., S. T., and V. W. S. acknowledge support from ARO Grant No. W911NF-16-1-0182. T. D. S. was supported by NSF Grant No. DMR-1414683. V. W. S. acknowledges support from AFOSR (FA9550-18-1-0505). C. Zhang is supported by NSF (PHY-1505496, PHY-1806227), ARO (W911NF-17-1-0128), and AFOSR (FA9550-16-1-0387).

[1] M. Z. Hasan and C. L. Kane, Rev. Mod. Phys. **82**, 3045 (2010).
[2] X.-L. Qi and S.-C. Zhang, Rev. Mod. Phys. **83**, 1057 (2011).
[3] W. A. Benalcazar, B. A. Bernevig, and T. L. Hughes, Science **357**, 61 (2017).
[4] W. A. Benalcazar, B. A. Bernevig, and T. L. Hughes, Phys. Rev. B **96**, 245115 (2017).
[5] Z. Song, Z. Fang, and C. Fang, Phys. Rev. Lett. **119**, 246402 (2017).
[6] F. Schindler, A. M. Cook, M. G. Vergniory, Z. Wang, S. S. P. Parkin, B. A. Bernevig, and T. Neupert, Sci. Adv. **4**, eaat0346 (2018).
[7] J. Langbehn, Y. Peng, L. Trifunovic, F. von Oppen, and P. W. Brouwer, Phys. Rev. Lett. **119**, 246401 (2017).
[8] L. Trifunovic and P. W. Brouwer, Phys. Rev. X **9**, 011012 (2019).
[9] M. Serra-Garcia, V. Peri, R. Ssstrunk, O. R. Bilal, T. Larsen, L. G. Villanueva, and S. D. Huber, Nature (London) **555**, 342 (2018).
[10] C. W. Peterson, W. A. Benalcazar, T. L. Hughes, and G. Bahl, Nature (London) **555**, 346 (2018).
[11] S. Imhof, C. Berger, F. Bayer, J. Brehm, L. W. Molenkamp, T. Kiessling, F. Schindler, C. H. Lee, M. Greiter, T. Neupert, and R. Thomale, Nat. Phys. **14**, 925 (2018).
[12] F. Schindler, Z. Wang, M. G. Vergniory, A. M. Cook, A. Murani, S. Sengupta, A. Y. Kasumov, R. Deblock, S. Jeon, I. Drozdov, H. Bouchiat, S. Guron, A. Yazdani, B. A. Bernevig, and T. Neupert, Nat. Phys. **14**, 918 (2018).
[13] Y. Wang, M. Lin, and T. L. Hughes, Phys. Rev. B **98**, 165144 (2018).
[14] Z. Yan, F. Song, and Z. Wang, Phys. Rev. Lett. **121**, 096803 (2018).
[15] Q. Wang, C.-C. Liu, Y.-M. Lu, and F. Zhang, Phys. Rev. Lett. **121**, 186801 (2018).
[16] A. Y. Kitaev, Phys. Usp. **44**, 131 (2001).
[17] L. Fu and C. L. Kane, Phys. Rev. Lett. **100**, 096407 (2008).
[18] X.-L. Qi, T. L. Hughes, and S.-C. Zhang, Phys. Rev. B **82**, 184516 (2010).
[19] K. T. Law, P. A. Lee, and T. K. Ng, Phys. Rev. Lett. **103**, 237001 (2009).
[20] J. D. Sau, R. M. Lutchyn, S. Tewari, and S. Das Sarma, Phys. Rev. Lett. **104**, 040502 (2010).
[21] C. Zhang, S. Tewari, R. M. Lutchyn, and S. Das Sarma, Phys. Rev. Lett. **101**, 160401 (2008).
[22] S. Tewari, S. Das Sarma, C. Nayak, C. Zhang, and P. Zoller, Phys. Rev. Lett. **98**, 010506 (2007).
[23] R. M. Lutchyn, J. D. Sau, and S. Das Sarma, Phys. Rev. Lett. **105**, 077001 (2010).
[24] M. Sato, Y. Takahashi, and S. Fujimoto, Phys. Rev. Lett. **103**, 020401 (2009).
[25] A. Cook and M. Franz, Phys. Rev. B **84**, 201105(R) (2011).
[26] A. R. Akhmerov, J. Nilsson, and C. W. J. Beenakker, Phys. Rev. Lett. **102**, 216404 (2009).
[27] E. Dumitrescu, J. D. Sau, and S. Tewari, Phys. Rev. B **90**, 245438 (2014).
[28] H. Hu, F. Zhang, and C. Zhang, Phys. Rev. Lett. **121**, 185302 (2018).
[29] X.-L. Qi, T. L. Hughes, S. Raghu, and S.-C. Zhang, Phys. Rev. Lett. **102**, 187001 (2009).
[30] F. Zhang, C. L. Kane, and E. J. Mele, Phys. Rev. Lett. **111**, 056402 (2013).
[31] C. L. M. Wong and K. T. Law, Phys. Rev. B **86**, 184516 (2012).
[32] F. Zhang, C. L. Kane, and E. J. Mele, Phys. Rev. Lett. **111**, 056403 (2013).
[33] F. Zhang and C. L. Kane, Phys. Rev. B **90**, 020501(R) (2014).
[34] X.-J. Liu, C. L. M. Wong, and K. T. Law, Phys. Rev. X **4**, 021018 (2014).
[35] F. Zhang and C. L. Kane, Phys. Rev. Lett. **113**, 036401 (2014).
[36] Z.-q. Bao and F. Zhang, Phys. Rev. Lett. **119**, 187701 (2017).
[37] C.-X. Liu and B. Trauzettel, Phys. Rev. B **83**, 220510(R) (2011).
[38] S. Nakosai, Y. Tanaka, and N. Nagaosa, Phys. Rev. Lett. **108**, 147003 (2012).
[39] S. Deng, L. Viola, and G. Ortiz, Phys. Rev. Lett. **108**, 036803 (2012).
[40] S. Nakosai, J. C. Budich, Y. Tanaka, B. Trauzettel, and N. Nagaosa, Phys. Rev. Lett. **110**, 117002 (2013).

[41] A. Keselman, L. Fu, A. Stern, and E. Berg, Phys. Rev. Lett. **111**, 116402 (2013).
[42] E. Gaidamauskas, J. Paaske, and K. Flensberg, Phys. Rev. Lett. **112**, 126402 (2014).
[43] J. Wang, Y. Xu, and S.-C. Zhang, Phys. Rev. B **90**, 054503 (2014).
[44] J. Klinovaja, A. Yacoby, and D. Loss, Phys. Rev. B **90**, 155447 (2014).
[45] C. Schrade, A. A. Zyuzin, J. Klinovaja, and D. Loss, Phys. Rev. Lett. **115**, 237001 (2015).
[46] Y. Huang and C.-K. Chiu, Phys. Rev. B **98**, 081412(R) (2018).
[47] J. C. Y. Teo and T. L. Hughes, Phys. Rev. Lett. **111**, 047006 (2013).
[48] R.-J. Slager, L. Rademaker, J. Zaanen, and L. Balents, Phys. Rev. B **92**, 085126 (2015).
[49] W. A. Benalcazar, J. C. Y. Teo, and T. L. Hughes, Phys. Rev. B **89**, 224503 (2014).
[50] Z. Wu, Z. Yan, and W. Huang, Phys. Rev. B **99**, 020508(R) (2019).
[51] C.-H. Hsu, P. Stano, J. Klinovaja, and D. Loss, Phys. Rev. Lett. **121**, 196801 (2018).
[52] M. Aidelsburger, M. Atala, M. Lohse, J. T. Barreiro, B. Paredes, and I. Bloch, Phys. Rev. Lett. **111**, 185301 (2013).
[53] P. G. Harper, Proc. Phys. Soc. London Sect. A **68**, 874 (1955).
[54] D. R. Hofstadter, Phys. Rev. B **14**, 2239 (1976).
[55] J. Struck, M. Weinberg, C. Ölschläger, P. Windpassinger, J. Simonet, K. Sengstock, R. Höppner, P. Hauke, A. Eckardt, M. Lewenstein, and L. Mathey, Nat. Phys. **9**, 738 (2013).
[56] H. Miyake, G. A. Siviloglou, C. J. Kennedy, W. C. Burton, and W. Ketterle, Phys. Rev. Lett. **111**, 185302 (2013).
[57] C. J. Kennedy, G. A. Siviloglou, H. Miyake, W. C. Burton, and W. Ketterle, Phys. Rev. Lett. **111**, 225301 (2013).
[58] D. Cocks, P. P. Orth, S. Rachel, M. Buchhold, K. Le Hur, and W. Hofstetter, Phys. Rev. Lett. **109**, 205303 (2012).
[59] G. Jotzu, M. Messer, R. Desbuquois, M. Lebrat, T. Uehlinger, D. Greif, and T. Esslinger, Nature (London) **515**, 237 (2014).
[60] L. Wang, H.-H. Hung, and M. Troyer, Phys. Rev. B **90**, 205111 (2014).
[61] M. Iskin, Phys. Rev. A **96**, 043628 (2017).
[62] R. O. Umucalılar and M. Iskin, Phys. Rev. Lett. **119**, 085301 (2017).
[63] H. P. Büchler, Phys. Rev. Lett. **104**, 090402 (2010).
[64] J. K. Chin, D. E. Miller, Y. Liu, C. Stan, W. Setiawan, C. Sanner, K. Xu, and W. Ketterle, Nature (London) **443**, 961 (2006).
[65] T. Bourdel, L. Khaykovich, J. Cubizolles, J. Zhang, F. Chevy, M. Teichmann, L. Tarruell, S. J. J. M. F. Kokkelmans, and C. Salomon, Phys. Rev. Lett. **93**, 050401 (2004).
[66] P.-I. Schneider and A. Saenz, Phys. Rev. A **87**, 052712 (2013).
[67] M. Antezza, F. Dalfovo, L. P. Pitaevskii, and S. Stringari, Phys. Rev. A **76**, 043610 (2007).
[68] T. Yefsah, A. T. Sommer, M. J. H. Ku, L. W. Cheuk, W. Ji, W. S. Bakr, and M. W. Zwierlein, Nature (London) **499**, 426 (2013).
[69] M. J. H. Ku, W. Ji, B. Mukherjee, E. Guardado-Sanchez, L. W. Cheuk, T. Yefsah, and M. W. Zwierlein, Phys. Rev. Lett. **113**, 065301 (2014).
[70] M. J. H. Ku, B. Mukherjee, T. Yefsah, and M. W. Zwierlein, Phys. Rev. Lett. **116**, 045304 (2016).
[71] J. Denschlag, Science **287**, 97 (2000).
[72] Y. Xu, L. Mao, B. Wu, and C. Zhang, Phys. Rev. Lett. **113**, 130404 (2014).
[73] X.-J. Liu, Phys. Rev. A **91**, 023610 (2015).
[74] S. Ryu, A. P. Schnyder, A. Furusaki, and A. W. W. Ludwig, New J. Phys. **12**, 065010 (2010).
[75] See Supplemental Material at http://link.aps.org/supplemental/10.1103/PhysRevLett.123.060402 for details of calculations and discussions of the connections with higher-order topological superconductors, which includes Refs. [61,62,72,73,76–81].
[76] X.-J. Liu, Phys. Rev. A **87**, 013622 (2013).
[77] Y. Xu, C. Qu, M. Gong, and C. Zhang, Phys. Rev. A **89**, 013607 (2014).
[78] C. Qu, M. Gong, and C. Zhang, Phys. Rev. A **89**, 053618 (2014).
[79] J. C. Y. Teo and C. L. Kane, Phys. Rev. B **82**, 115120 (2010).
[80] Z. Yan, R. Bi, and Z. Wang, Phys. Rev. Lett. **118**, 147003 (2017).
[81] C. Chan, L. Zhang, Ting Fung Jeffrey Poon, Y.-P. He, Y.-Q. Wang, and X.-J. Liu, Phys. Rev. Lett. **119**, 047001 (2017).
[82] M. Aidelsburger, M. Lohse, C. Schweizer, M. Atala, J. T. Barreiro, S. Nascimbne, N. R. Cooper, I. Bloch, and N. Goldman, Nat. Phys. **11**, 162 (2015).
[83] M. Iskin, Phys. Rev. A **91**, 053606 (2015).
[84] R. A. Williams, M. C. Beeler, L. J. LeBlanc, K. Jiménez-García, and I. B. Spielman, Phys. Rev. Lett. **111**, 095301 (2013).
[85] C. Nayak, S. H. Simon, A. Stern, M. Freedman, and S. Das Sarma, Rev. Mod. Phys. **80**, 1083 (2008).
[86] C. Zhang, V. W. Scarola, S. Tewari, and S. Das Sarma, Proc. Natl. Acad. Sci. U.S.A. **104**, 18415 (2007).